Robotica (2018) volume 36, pp. 1454–1476. © Cambridge University Press 2018
doi:10.1017/S0263574718000498

A reconfigurable tri-prism mobile robot with eight modes

Jieyu Wang†,*, Yan'an Yao‡,** and Xianwen Kong†

†*School of Engineering and Physical Sciences, Heriot-Watt University, Edinburgh EH14 4AS, UK. E-mail: x.kong@hw.ac.uk*
‡*School of Mechanical, Electronic and Control Engineering, Beijing Jiaotong University, Beijing 100044, P.R. China*

(Accepted May 25, 2018. First published online: June 27, 2018)

SUMMARY
A novel reconfigurable tri-prism mobile robot with eight modes is proposed. The robot is composed of two feet connected by three U-R-U (universal-revolute-universal) limbs. The robot incorporates the kinematic properties of sphere robots, squirming robots, tracked robots, wheeled robots and biped robots. In addition, the somersaulting and turning modes are also explored. After the description of the robot, the DOF (degree-of-freedom) is calculated based on screw theory. The 3D model and simulations indicate that the robot can cross several typical obstacles and can also be folded via two approaches. Finally, the prototype experiments are presented to verify the feasibility of the proposed mobile robot in different motion mode.

KEYWORDS: Mobile robot, Reconfigurable robot, Obstacle crossing, Foldable robot, Screw theory

1. Introduction

Typical single-mode mobile robots mainly include biped robots, sphere robots, wheeled robots, squirming robots and tracked robots. Biped robots have the merit of walking on the terrain with discrete obstacles.[1–3] Sphere robots can roll on the rugged ground and do not tumble.[4–6] Wheeled robots usually work in the subdued topography with high speed and stability.[7] Squirming robots have a superior capability in narrow environments, such as gully region.[8–10] Tracked robots are widely used in the field with loose sand.[11] However, each category of mobile robots has its own limitations, single-mode robots cannot adapt to much more complex and unknown environments.

In order to meet the requirements of various tasks, a number of robots with multiple modes have been proposed. One of the approaches that achieve reconfigurability is combining two or more robots with single mode,[12–20] but these robots tend to be heavy and bulky. Another method is to accomplish transitions by disassembling and reassembling modules. Yim[21] put forward the concept of the self-reconfigurable robot, of which the locomotion modes can be switched among rolling, crawling and walking. The idea was also applied in a metamorphic robotic system.[22] However, self-reconfiguration robots have very large DOF (degree-of-freedom) and are not easy to control.

In refs. [23-25], single-mode mobile robots, such as a planar 4R linkage, which rolls along a straight line, a spherical 4R linkage, which rolls along a polygon, 4U biped robot and 6U rolling robots were constructed. Meanwhile, some parallel robots, such as Stewart platform, Delta mechanism and 3-RPC parallel mechanism were used for mobile robots.[26–28] However, all of these robots have single mode and can only move along one type of trajectory. In order to improve the mobile capability of the mobile robots in different environments, it is required to develop novel mobile robots with multiple modes. Inspired by recent advances in disassembly-free reconfigurable mechanisms,[29–35] several mobile robots with multiple modes were investigated. Zhang[36] put forward a six-bar spherical metamorphic mechanism used in the body design of a rover mechanism. A biped walking robot on

* Corresponding author. E-mail: jw26@hw.ac.uk
**Corresponding author. E-mail: yayao@bjtu.edu.cn

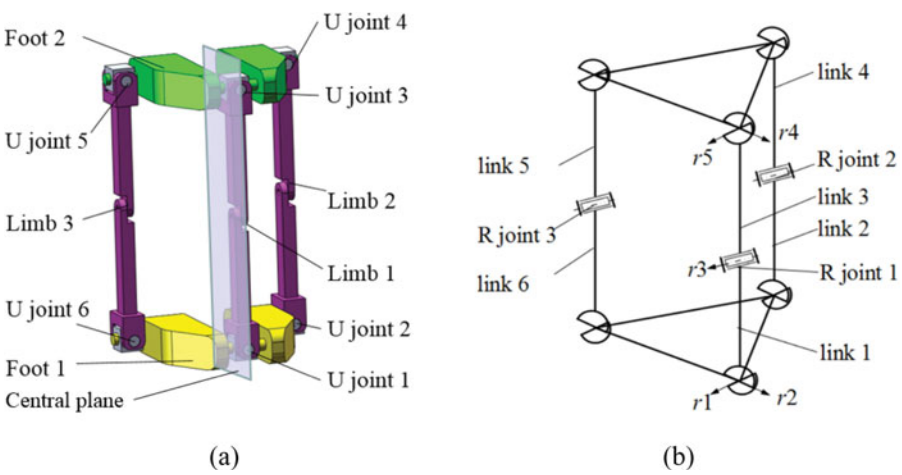

Fig. 1. Mechanism design of the mobile robot: (a) 3D model of the robot; (b) sketch of the robot.

the basis of a spatial eight-bar kinematotropic mechanism was proposed in ref. [37]. Metamorphic hybrid wheel-legged rover was investigated by Ding.[38] Dai[39] developed a discontinuous-constraint metamorphic mechanism for a gecko-like robot. Tian[40] constructed a mobile eight-bar linkage that can roll along a straight line as well as a polygon. Wang[41] designed a rolling robot that can switch modes between planar linkage mode and spherical linkage mode by folding and spreading.

This paper aims to propose a novel reconfigurable tri-prism mobile robot with eight modes. The robot integrates the motion characteristics of biped robots, sphere robots, wheeled robots, squirming robots and tracked robots into a single robot to adapt to different kinds of environments, such as those in cases of planet explorations and earthquake search and rescue.

This paper is organized as follows. The mechanism design is presented in Section 2. Section 3 discusses the DOF analysis of the mobile robot. Section 4 covers the motion modes analysis. Section 5 provides several experiments of a physical prototype. The conclusions are drawn in Section 6.

2. Mechanism Design

The mobile robot consists of three U-R-U (universal- revolute-universal) limbs and two feet (Fig. 1). Each limb is comprised of two RU links. For convenience, all the R joints, including those within U joints, in a limb are numbered $r1$, $r2$, $r3$, $r4$ and $r5$ starting from foot 1 to foot 2 [see Fig. 1(b)]. In the reference configuration, limbs 1 and 3 are symmetrical about the central plane of the robot, and limb 2 is located on the central plane. In the initial state, the axes of joints $r1$, $r3$ and $r5$ in all the limbs are parallel, and those of joints $r2$ and $r4$ in all the limbs are parallel as well. The robot is singular in this configuration.

A prototype is designed as shown in Fig. 2. The feet and the links are made of plastic to reduce the weight of the robot, while the shafts are manufactured with aluminum to ensure the strength of the prototype.

3. DOF Analysis

As shown in Fig. 3, a coordinate system is attached to universal joint 1, x-axis and y-axis are along the two axes of the universal joint 1 respectively, and z-axis can be obtained by the right-hand rule.

In a general configuration, the DOF of the mobile robot is calculated as three, according to the conventional formula.[42] The detailed analysis can be found in the supplementary materials A.

The proposed mobile robot has four configurations and can switch configurations by changing actuation modes. When operates in Configuration I, the robot has five motion modes, including sphere rolling motion, tracked rolling motion, squirming motion, biped walking motion and folding function. The other three configurations each has one mobile mode, namely wheeled rolling motion, somersauting motion and turning motion. The DOFs and geometric characteristics of the mobile robot in the eight modes are listed in Table I.

https://doi.org/10.1017/S0263574718000498 Published online by Cambridge University Press

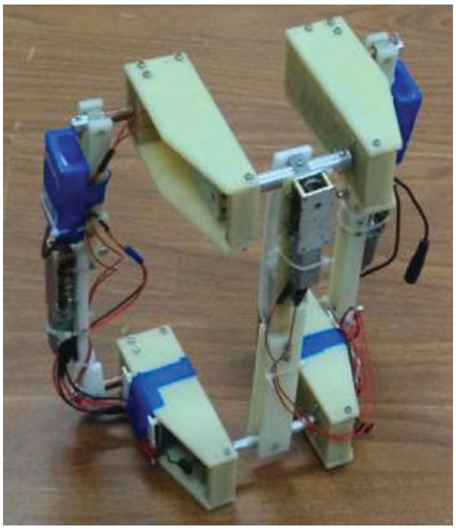

Fig. 2. The prototype of the mobile robot.

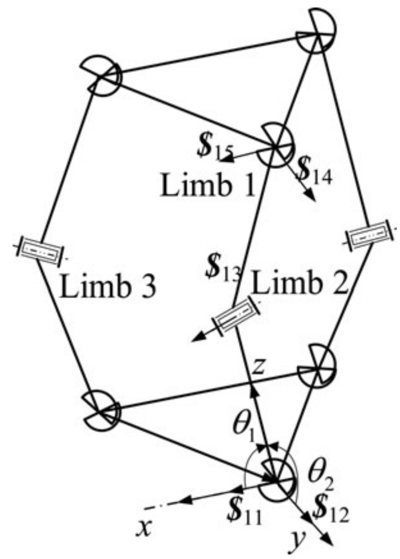

Fig. 3. DOF analysis of the mobile robot.

The four configurations and eight motion modes will be detailed in Section 4. Due to the multi-mode nature of the mobile robot (Fig. 4), five motors $M1$, $M1$', $M2$, $M3$ and $M4$ are set to control the robot in different configurations. $M1$ and $M1$' are assembled on R joint $r3$ in limb 3 and R joint $r3$ in limb 2, respectively, and are driven synchronously; $M2$, $M3$ and $M4$ are mounted on $r5$, $r1$ and $r2$ of limb 1, respectively. It is noted that apart from the eight modes in which the driving angles of $M1$ and $M1$' are equal, there exist theoretical motion modes in which the angles of $M1$ and $M1$' are distinct. To identify these theoretical motion modes is out of the scope of this paper. The detailed DOF analysis of each configuration using screw theory (see refs. [43] and [44] for example) is given as follows.

3.1. Configuration I

When the axes of joints $r1$, $r3$ and $r5$ in all the limbs are parallel, lock $M4$, then the robot turns to Configuration I (see the first row of Table I). Joints $r2$ and $r4$ in all the limbs lose their DOFs. For the sake of convenience of calculation, $r2$ and $r4$ in all the limbs are locked, the twist system of limb 1

https://doi.org/10.1017/S0263574718000498 Published online by Cambridge University Press

Table I. Motion modes of the eight-mode mobile robot.

Configuration	Degree of freedom	Description	Mode		
I	*F=3*	When all the axes of joints $r1$, $r3$ and $r5$ in all the limbs are parallel, lock $M4$. Joints $r2$ and $r4$ in all the limbs lose their DOFs.	I	Sphere rolling motion	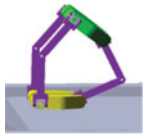
			II	Tracked rolling motion	
			III	Squirming motion	
			IV	Biped walking motion	
			V	Folding function	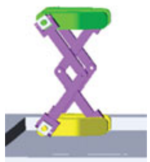
II	*F=1*	When all the axes of joints $r1$, $r3$ and $r5$ in all the limbs are parallel, so are $r2$ and $r4$, lock $M1$ and $M4$, and drive $M2$ and $M3$ with the same direction and velocity. Joints $r2$, $r3$ and $r4$ in all the limbs lose their DOFs.	VI	Wheeled rolling motion	
III	*F=1*	When all the axes of joints $r1$, $r3$ and $r5$ in all the limbs are parallel, link 1 is perpendicular to foot 1 and link 3 is perpendicular to foot 2, lock $M2$, $M3$ and $M4$. Joints $r2$ and $r4$ in all the limbs, as well as $r1$ and $r5$ in limb 1 lose their DOFs.	VII	Somersauting motion	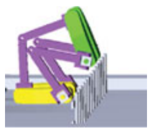
IV	*F=2*	When all the axes of joints $r1$, $r3$ and $r5$ in all the limbs are parallel, as well as $r2$ and $r4$, lock $M1$, and drive $M2$ and $M3$ with the same direction and velocity. Joints $r3$ in all the limbs lose their DOFs.	VIII	Turning motion	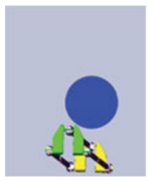

is expressed as

$$\begin{aligned} \$_{11} &= (1 \;\; 0 \;\; 0\,;\; 0 \;\; 0 \;\; 0) \\ \$_{13} &= (1 \;\; 0 \;\; 0\,;\; 0 \;\; -z_{12} \;\; 0) \\ \$_{15} &= (1 \;\; 0 \;\; 0\,;\; 0 \;\; -z_{13} \;\; y_{13}) \end{aligned} \tag{1}$$

https://doi.org/10.1017/S0263574718000498 Published online by Cambridge University Press

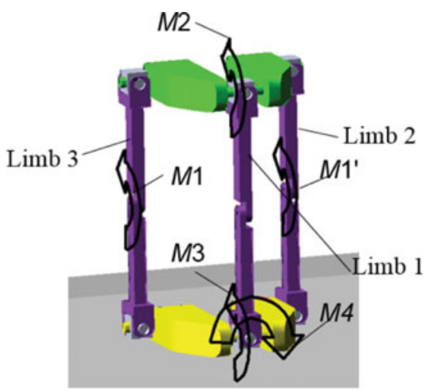

Fig. 4. Simulation model of the mobile robot.

The wrench system of limb 1 can be derived as

$$\begin{aligned} \$^r_{11} &= (0\ \ 0\ \ 0;\ \ 0\ \ 0\ \ 1) \\ \$^r_{12} &= (1\ \ 0\ \ 0;\ \ 0\ \ 0\ \ 0) \\ \$^r_{13} &= (0\ \ 0\ \ 0;\ \ 0\ \ 1\ \ 0) \end{aligned} \tag{2}$$

The twist system of limb 2 is

$$\begin{aligned} \$_{11} &= (1\ \ 0\ \ 0\ ;\ 0\ \ \ -z_{21}\ \ y_{21}) \\ \$_{13} &= (1\ \ 0\ \ 0\ ;\ 0\ \ \ -z_{22}\ \ y_{22}) \\ \$_{15} &= (1\ \ 0\ \ 0\ ;\ 0\ \ \ -z_{23}\ \ y_{23}) \end{aligned} \tag{3}$$

The wrench system of limb 2 can be calculated as

$$\begin{aligned} \$^r_{21} &= (0\ \ 0\ \ 0;\ \ 0\ \ 0\ \ 1) \\ \$^r_{22} &= (1\ \ 0\ \ 0;\ \ 0\ \ 0\ \ 0) \\ \$^r_{23} &= (0\ \ 0\ \ 0;\ \ 0\ \ 1\ \ 0) \end{aligned} \tag{4}$$

$\$^r_{11}$ and $\$^r_{21}$ represent couple wrenches parallel to axis z, $\$^r_{12}$ and $\$^r_{22}$ are force wrenches coincident with axis x. and $\$^r_{13}$ and $\$^r_{23}$ are couple wrenches about y-axis. Limb 3 has the same type of constraint with limb 1 and 2. The total constraints exerted on the foot 2 are equivalent to one constraint force in direction of x-axis and constraint couples about y-axis and z-axis. Consequently, the robot has two translational DOFs along y-axis and z-axis and one rotational DOF about x-axis, i.e., 2T1R.

3.2. Configuration II

In order to let the mobile robot operate in Configuration II (see the second row of Table I), lock $M1$ and $M4$ and drive $M2$ and $M3$ with the same direction and velocity when the axes of joints $r1$, $r3$ and $r5$ in all the limbs are parallel, as well as $r2$ and $r4$. In configuration II, joints $r2$, $r3$ and $r4$ in all the limbs lose their DOFs.

The twist system of limb 1 is given by

$$\begin{aligned} \$_{11} &= (1\ \ 0\ \ 0\ ;\ 0\ \ 0\ \ 0) \\ \$_{15} &= (1\ \ 0\ \ 0\ ;\ 0\ \ \ -z_{13}\ \ 0) \end{aligned} \tag{5}$$

The wrench system of limb 1 can be derived as

$$\begin{aligned} \$^r_{11} &= (0\ \ 0\ \ 1;\ \ 0\ \ 0\ \ 0) \\ \$^r_{12} &= (0\ \ 0\ \ 0;\ \ 0\ \ 0\ \ 1) \\ \$^r_{13} &= (1\ \ 0\ \ 0;\ \ 0\ \ 0\ \ 0) \\ \$^r_{14} &= (0\ \ 0\ \ 0;\ \ 0\ \ 1\ \ 0) \end{aligned} \tag{6}$$

https://doi.org/10.1017/S0263574718000498 Published online by Cambridge University Press

The three limbs of the robot have identical structure and the same type of constraints in this configuration. As a result, the total constraints exerted on foot 2 are equivalent to constraint forces along x-axis and z-axis, and couples about x-axis, y-axis and z-axis. The robot in this mode only has one translational DOF along y-axis.

3.3. Configuration III

When the axes of joints $r1$, $r3$ and $r5$ in all the limbs are parallel, link 1 is perpendicular to foot 1 and link 3 is perpendicular to foot 2, lock $M2$, $M3$ and $M4$. Then, the mobile robot is in Configuration III (as shown in the third row of Table I). In configuration III, joints $r2$ and $r4$ in all the limbs, as well as $r1$ and $r5$ in limb 1 lose their DOFs.

The twist of limb 1 is obtained as

$$\$_{13} = (1 \;\; 0 \;\; 0\,; \;\; 0 \;\; -z_{21} \;\; 0) \tag{7}$$

The wrench system of limb 1 is derived as

$$\begin{aligned} \$^r_{21} &= (0 \;\; 0 \;\; 1; \;\; 0 \;\; 0 \;\; 0) \\ \$^r_{22} &= (0 \;\; 1 \;\; 0; \;\; z_{21} \;\; 0 \;\; 0) \\ \$^r_{23} &= (1 \;\; 0 \;\; 0; \;\; 0 \;\; 0 \;\; 0) \\ \$^r_{24} &= (0 \;\; 0 \;\; 0; \;\; 0 \;\; 0 \;\; 1) \\ \$^r_{25} &= (0 \;\; 0 \;\; 0; \;\; 0 \;\; 1 \;\; 0) \end{aligned} \tag{8}$$

The twist system of limb 2 can be got as

$$\begin{aligned} \$_{11} &= (1 \;\; 0 \;\; 0\,; \;\; 0 \;\; -z_{21} \;\; y_{21}) \\ \$_{13} &= (1 \;\; 0 \;\; 0\,; \;\; 0 \;\; -z_{22} \;\; y_{22}) \\ \$_{15} &= (1 \;\; 0 \;\; 0\,; \;\; 0 \;\; -z_{23} \;\; y_{23}) \end{aligned} \tag{9}$$

The wrench system of limb 2 is calculated as

$$\begin{aligned} \$^r_{21} &= (0 \;\; 0 \;\; 0; \;\; 0 \;\; 0 \;\; 1) \\ \$^r_{22} &= (1 \;\; 0 \;\; 0; \;\; 0 \;\; 0 \;\; 0) \\ \$^r_{23} &= (0 \;\; 0 \;\; 0; \;\; 0 \;\; 1 \;\; 0) \end{aligned} \tag{10}$$

Limb 3 has the same type of constraint with limb 2. Hence, the total constraints of foot 2 are forces along x-axis, y-axis and z-axis, and couples about y-axis and z-axis. The robot in this mode only has one rotational DOF about x-axis.

3.4. Configuration IV

In Configuration IV (fourth row of Table I), lock $M1$ and drive $M2$ and $M3$ with the same direction and velocity when all the axes of joints $r1$, $r3$ and $r5$ in all the limbs are parallel, as well as $r2$ and $r4$. Joints $r3$ in all the limbs lose their DOFs. The twist system of limb 1 is

$$\begin{aligned} \$_{11} &= (1 \;\; 0 \;\; 0\,; \;\; 0 \;\; 0 \;\; 0) \\ \$_{12} &= (0 \;\; 1 \;\; 0\,; \;\; 0 \;\; 0 \;\; 0) \\ \$_{14} &= (0 \;\; 1 \;\; 0\,; \;\; z_{13} \;\; 0 \;\; -x_{13}) \\ \$_{15} &= (1 \;\; 0 \;\; 0\,; \;\; 0 \;\; -z_{13} \;\; 0) \end{aligned} \tag{11}$$

The wrench system of limb 1 can be derived as

$$\begin{aligned} \$^r_{11} &= (0 \;\; 0 \;\; 1; \;\; 0 \;\; 0 \;\; 0) \\ \$^r_{12} &= (0 \;\; 0 \;\; 0; \;\; 0 \;\; 0 \;\; 1) \end{aligned} \tag{12}$$

$\$_{11}$ and $\$^r_{12}$present forces along z-axis and couples about z-axis, respectively. The three limbs have identical type of constraints, so the wrench system of the foot 2 consists of couples about x-axis, y-axis

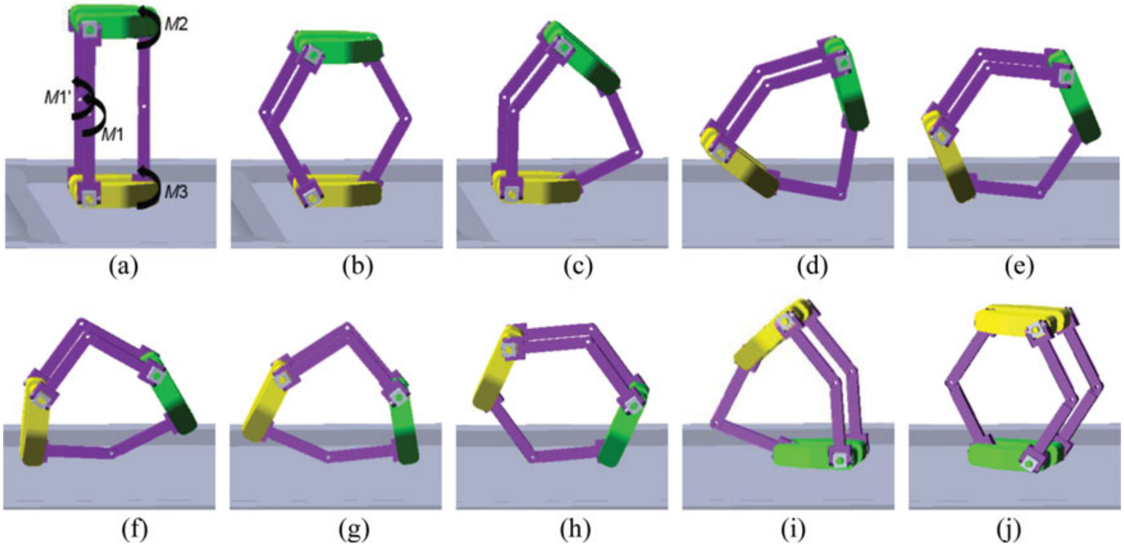

Fig. 5. Sphere rolling motion.

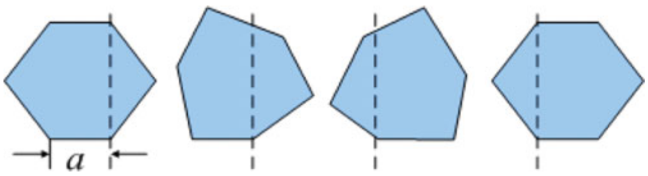

Fig. 6. The step size of the mobile robot in the sphere rolling mode.

and z-axis and a force along z-axis. Therefore, the robot has two translational DOFs along x-axis and y-axis, namely, 2T.

4. Motion Mode Analysis

In this section, several simulations are carried out to verify the function of obstacle negotiation of the mobile robot. Kinematic analysis and stability analysis are also given. Let θ_1 and θ_2 be the angle between link 1 and x-axis and that between link 1 and y-axis, respectively (Fig. 3). For brevity reasons, only the first step of the mobile motion, when foot 1 touches the ground is calculated. Let a be the length of link 1, as well as the distance between U joint 1 and U joint 6. l is the thickness of the foot.

4.1. Sphere rolling motion

The robot is in Configuration I when working in the sphere rolling mode (mode I in Table I). At the beginning of rolling motion, the projection view on yz plane of the mobile robot is in the shape of regular hexagon and the robot moves as a closed-loop six-bar planar linkage.

4.1.1. Gait analysis. When the robot operates in the sphere rolling mode (Fig. 5), lock $M4$, drive $M1$, $M2$ and $M3$ clockwise. After turning to the posture presented in Fig. 5(b), reverse the direction of $M1$ and drive $M1$, $M2$ and $M3$ with the same angles, then the robot deforms into the posture shown in Fig. 5(c). The robot tips over due to the inertia forces and moments [Fig. 5(d)] and can turn to the posture in Fig. 5(e) when changing the rotation direction of $M1$, $M2$ and $M3$. The motion is inspired by the animal motion of tumble down hills. The merit of this mode is that the robot can operate on slopes and achieve shift quickly. The rolling motion is similar to the sphere robot, so the mode is named sphere rolling mode. The difference is the tri-prism mobile robot touches the ground by line or plane contact, whereas sphere robots roll via point contact with the ground. The size of each step of the mobile robot in the sphere rolling mode is a, as shown in Fig. 6.

https://doi.org/10.1017/S0263574718000498 Published online by Cambridge University Press

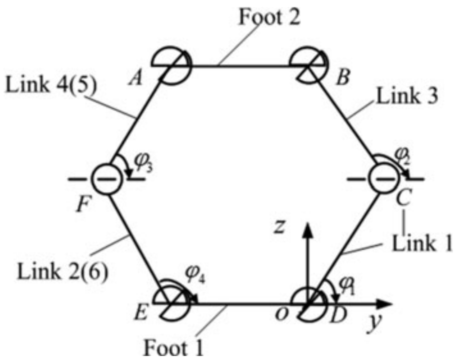

Fig. 7. The projection view on *yz* plane of the mobile robot in the sphere rolling mode.

4.1.2. Stability analysis. The projection view on *yz* plane of the mobile robot is in the shape of hexagon. As shown in Fig. 7, φ_1 ($\varphi_1 = \theta_2$), φ_2, φ_3 and φ_4 represent the angles between *xy* plane and link 1, link 3, link 5 and link 6, respectively. According to the calculation, φ_2 is always equal to $2\pi/3$, $\varphi_3 = \pi/3$ and $\varphi_4 = \pi/3+\varphi_1$ before tipping over [Fig. 6(a–c)], since the interval interior angles of the hexagon are always equal ($\angle FAB = \angle BCD = \angle DEF$). The position of each link and foot is calculated, which can be found in supplementary material B.

In this paper, ZMP (zero moment point)[45] is used to investigate the conditions for the robot to achieve rolling motion. The coordinates of ZMP are expressed as

$$x_{zmp} = \frac{\sum_{i=0}^{n} [m_i x_i(\ddot{z}_i + g) - m_i z_i \ddot{x}_i]}{\sum_{i}^{n} m_i(\ddot{z}_i + g)} \tag{13}$$

$$y_{zmp} = \frac{\sum_{i=0}^{n} [m_i y_i(\ddot{z}_i + g) - m_i z_i \ddot{y}_i]}{\sum_{i}^{n} m_i(\ddot{z}_i + g)} \tag{14}$$

where m_i, (x_i, y_i, z_i) and $(\ddot{x}_i, \ddot{y}_i, \ddot{z}_i)$ denote, respectively, the mass, the position of the CM (center of mass), and the acceleration of the CM of the *i*th link. *g* is the gravitational acceleration.

The values of θ_1 and x_{zmp} of the robot operating in the sphere rolling mode are equal to zero. The acceleration of the motor α is defined as zero, which means the motors rotate at constant angular velocity. Replacing φ_4 and φ_1 with the function of θ_2, and deriving the acceleration of each link (see in supplementary material B), then the position of y_{zmp} is calculated as

$$y_{zmp} = \frac{-12ag(9 - 7\cos\theta_2 + 3\sqrt{3}\sin\theta_2) + a\omega^2[\sqrt{3}(3 + 17a) + 6\sqrt{3}(3 + 2a)\cos\theta_2 - 6\sqrt{3}(a - 1)\cos 2\theta_2 + 6(10a - 3)\sin\theta_2]}{192g - 12a\omega^2(3\sqrt{3} + 3\sqrt{3}\cos\theta_2 + 7\sin\theta_2)} \tag{15}$$

When y_{zmp} goes beyond the support area, the robot will tumble. The rolling condition is

$$\begin{aligned} &y_{zmp} \leq -a \text{ or} \\ &y_{zmp} \geq 0 \end{aligned} \tag{16}$$

Suppose that $a = 0.1$m, the mass of the links $m_1 = 0.1$kg, and the mass of the feet $m_2 = 0.3$kg. We define $\omega = \pi$ rad/s, θ_2 can be calculated as

$$\begin{aligned} \theta_2 &\leq 16.31^\circ \text{ or} \\ \theta_2 &\geq 86.85^\circ \end{aligned} \tag{17}$$

https://doi.org/10.1017/S0263574718000498 Published online by Cambridge University Press

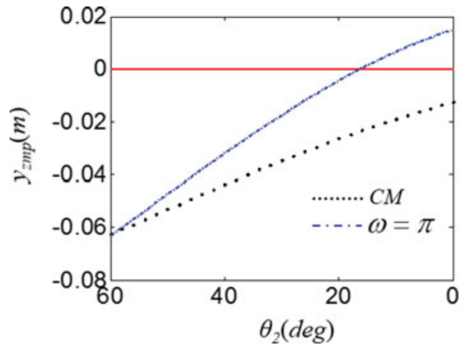

Fig. 8. Plot of ZMP in the sphere rolling mode.

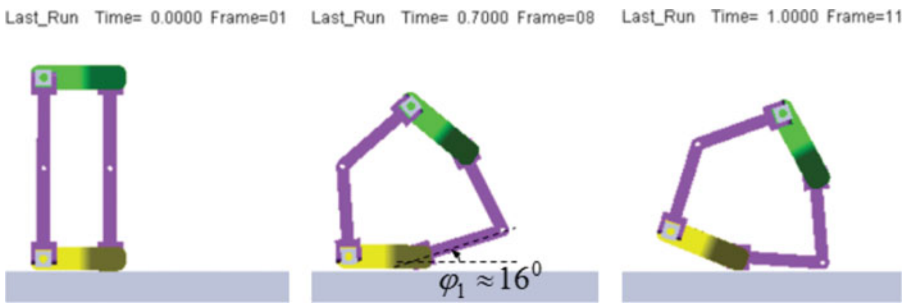

Fig. 9. Simulation result of the mobile robot in the sphere rolling mode.

The result can be verified by both the plot of y_{zmp} vs. θ_2 obtained using MATLAB^{TM} (Fig. 8), and the simulation with ADAMS^{TM} (Fig. 9).

4.2. Tracked rolling motion

The robot is capable of undergoing tracked rolling motion (mode II in Table I), as shown in Fig. 10. The projection view on *yz* plane of the mobile robot remains the shape of a parallelogram during rolling motion.

To begin with, $M1$ is immobilized, $M2$ rotates anticlockwise and $M3$ rotates clockwise. The robot tumbles when the position of ZMP goes beyond of the supporting area, as shown in Fig. 10(c). Then, the robot can either roll in the shape of a normal parallelogram, as shown in Fig. 10(d–g) or in the shape of rectangle in Fig. 10(h–k). Repeating the process above, the robot can realize continuous rolling longitudinally. The robot in this mode acts the same way with tracked robot and can run on soft sand or other rough roads.

As shown in Fig. 11, the length of each step of the robot in the tracked rolling mode is *a*.

4.3. Squirming motion

When encountering the height restrictions, the robot evolves into the squirming mode (mode III in Table I), as shown in Fig. 12. In the initial state, the robot spreads with two feet touching the ground.

The robot achieves squirming motion based on the principle of difference between friction forces. In order to make the friction force between one foot and the ground different from the other foot and the ground, one foot needs to be inclined, as shown in Fig. 12(b). At the outset of the motion, lift one end of foot 2 and extend the robot, then bend the body to let foot 1 move forward. The motion of squirming is alike the moving step of an inchworm, which moves by looping the body in alternate contractions and expansions.

The gait is also similar to soldiers' creeping forward. The mode is used to across the obstacles with a height limit of $\sqrt{3}a/2$, as shown in Fig. 13.

https://doi.org/10.1017/S0263574718000498 Published online by Cambridge University Press

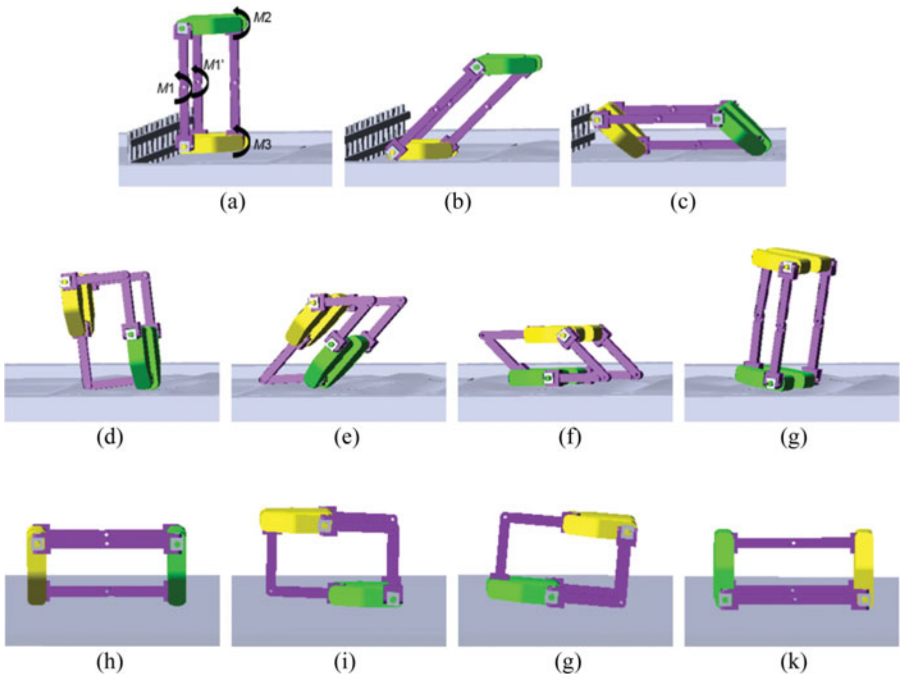

Fig. 10. Tracked rolling motion.

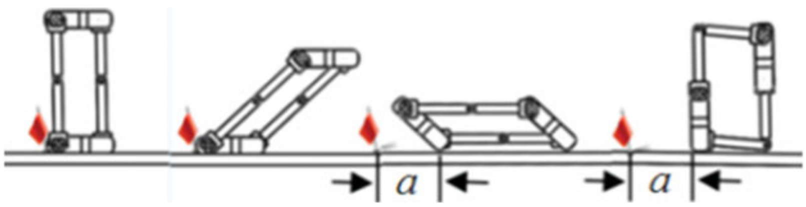

Fig. 11. The step length of the mobile robot in the tracked rolling mode.

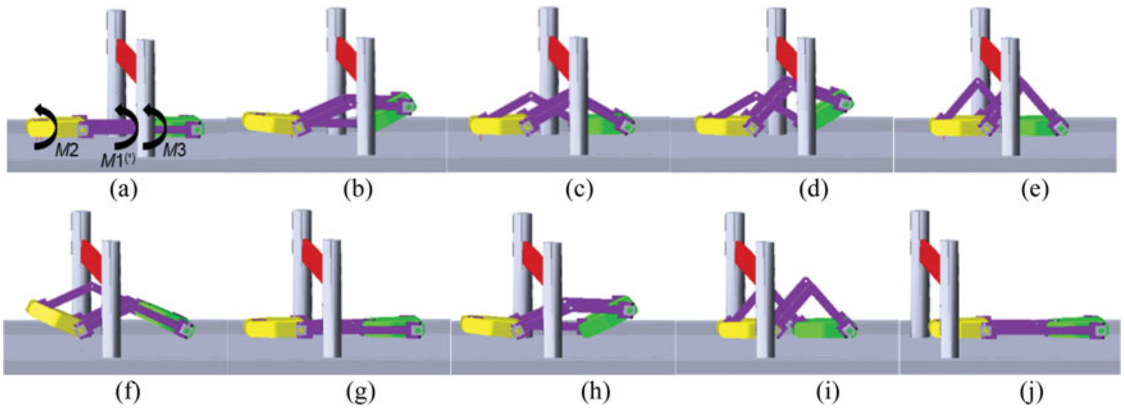

Fig. 12. Squirming motion.

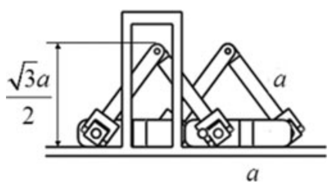

Fig. 13. Height limit of the mobile robot in the squirming mode.

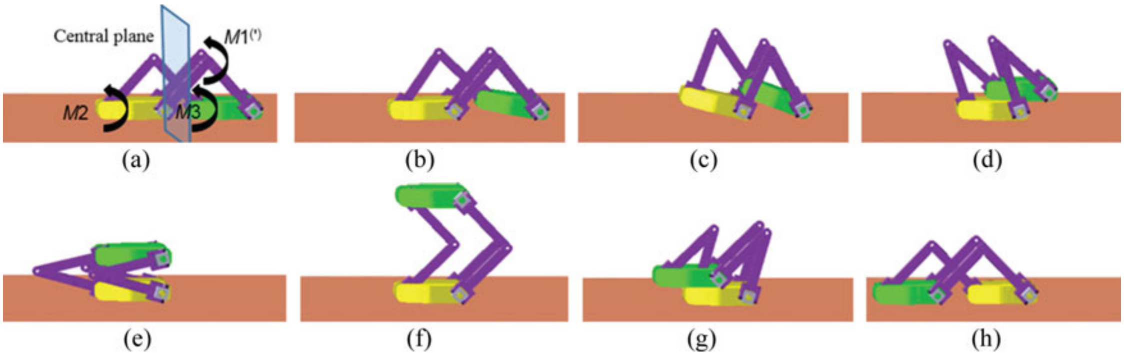

Fig. 14. Biped walking motion.

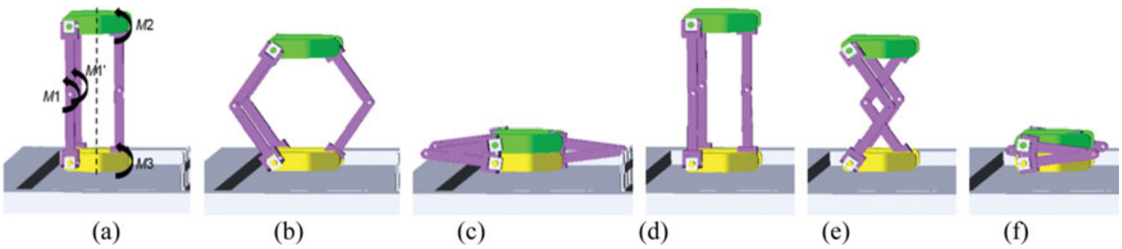

Fig. 15. Folding function.

4.4. Biped walking motion

The process of biped walking motion (mode IV in Table I) is shown in Fig. 14. Similar to the squirming mode, the robot is spread in the initial state.

Unlike the right and left feet robot, the robot in this paper is arranged as front and back structure. In the biped walking mode, one of the feet cannot entirely lift by itself considering the robot is symmetrically distributed with respect to the central plane [Fig. 14(a)]. After lifting foot 1 with the support of foot 2 [Fig. 14(b–e)], lay down foot 2 to accomplish a cycle of walking motion. In the squirming mode, the feet do not need to be lifted so it is more energy-efficient, but the pace is smaller than the robot in the biped walking mode.

4.5. Folding function

The robot can be folded via two approaches (mode V in Table I), as shown in Fig. 15. The two feet are always parallel, and the projection view on yz plane of the mobile robot is bilaterally symmetrical about the central line [Fig. 15(a)] during this process.

Locking $M4$, driving $M2$ and $M3$ to rotate by ζ [$\zeta = \arccos(l/2a)$] and $M1$ to rotate by 2ζ, the robot can be alternatively folded into the posture in Fig. 15(c) or Fig. 15(f).

The minimum height of the robot $h_1 = 2l$ [Fig. 15(c) and (f)] and the maximum height of the robot $h_2 = 2a + l$ [Fig. 15(a)], without consideration of interference of the mechanism.

The merits of the folding function are as follows: (1) elusive: hiding when encountering emergency; and (2) portable: saving space to facility storage and transportation. The robot can also serve as a lift in the folding mode.

4.6. Wheeled rolling motion

The mobile robot operates in the wheeled rolling mode (mode VI in Table I) is in Configuration II.

4.6.1. Gait analysis. The robot has the ability of going up and down stairs by operating in the wheeled rolling mode, as presented in Fig. 16. In order to enable the limbs to have complete revolution and the two feet to achieve successive rolling, the foot is designed as two prismatoids connected by a shaft instead of one prism, and the limbs are assembled on the shaft and both sides of the feet.

Actuating $M3$ to rotate clockwise, until the position of ZMP goes beyond the supporting area and the robot begins to roll, as shown in Fig. 16(c). Then, continue to drive $M3$ to rotate to achieve rolling motion. The two feet rolls in the same way as two wheels, and the gait has the identical characteristics

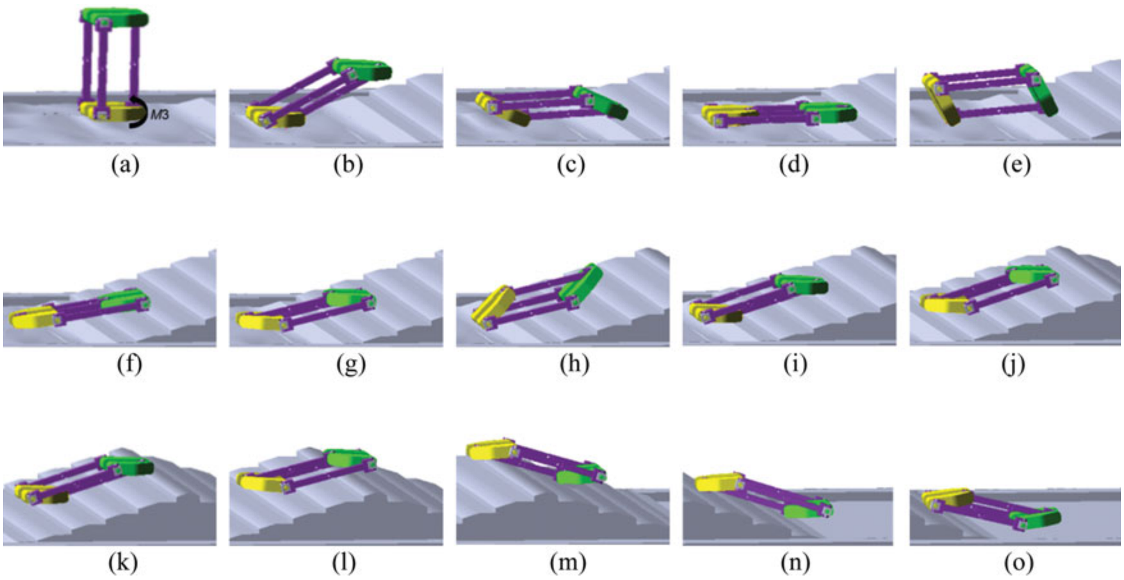

Fig. 16. Wheeled rolling mode.

of the wheeled robot. Hence, the mode is called wheeled rolling mode. Unlike the general wheeled robot, the wheels of the tri-prism mobile robot are in the shape of rectangle and rotate about a virtual axis. Since the directions of the motors do not have to be changed during the rolling motion, the robot in this mode can achieve fast motion.

4.6.2. Stability analysis. Calculating the position of each link and foot, and deriving the second-order derivative (in supplementary material C) and substituting them into Eqs. (13) and (14), the position of ZMP can be obtained. In the wheeled rolling mode, $x_{zmp} = 0$, y_{zmp} of the robot can be obtained as

$$y_{zmp} = \frac{a[3g\cos\theta_2 + \sqrt{3}(-g + a\omega_2{}^2\sin\theta_2)]}{3(g - a\omega_2{}^2\sin\theta_2)} \tag{18}$$

The supporting area of the robot along y-axis is $[-a, 0]$. When ZMP goes beyond the supporting area, the robot will turn over. The rolling condition is

$$\begin{array}{l} y_{zmp} \leq -a \quad \text{or} \\ y_{zmp} \geq 0 \end{array} \tag{19}$$

Let $\omega = \pi$, the scale of θ_2 can be obtained as

$$\begin{array}{lcl} \theta_2 & \leq & 58.16^\circ \quad \text{or} \\ \theta_2 & \geq & 112.59^\circ \end{array} \tag{20}$$

Figure 17 gives the ZMP of the robot in the wheeled rolling mode when $\omega = \pi$ and the CM of the robot. The robot will flip over with the actuator rotating specific angle with arbitrary ω, and it rolls more easily with the increase of ω.

In the simulation, the robot tips over when $\theta_2 \approx 113^\circ$ (Fig. 18), which confirms that the calculation above is correct.

The input and the displacement and velocity of CM of foot 2 in the simulation using ADAMS are given in Fig. 19. As shown in Fig. 20, the rolling cycle begins at the first second and ends at the third second, and the moving distance in one cycle is about 272.5 mm.

https://doi.org/10.1017/S0263574718000498 Published online by Cambridge University Press

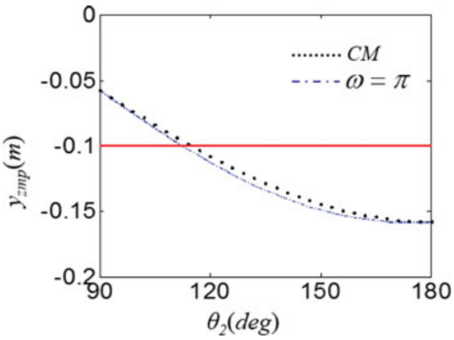

Fig. 17. Plot of ZMP in the wheeled rolling mode.

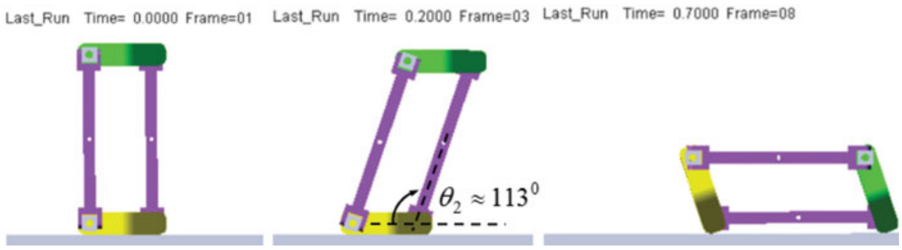

Fig. 18. Simulation result of ZMP in the wheeled rolling mode.

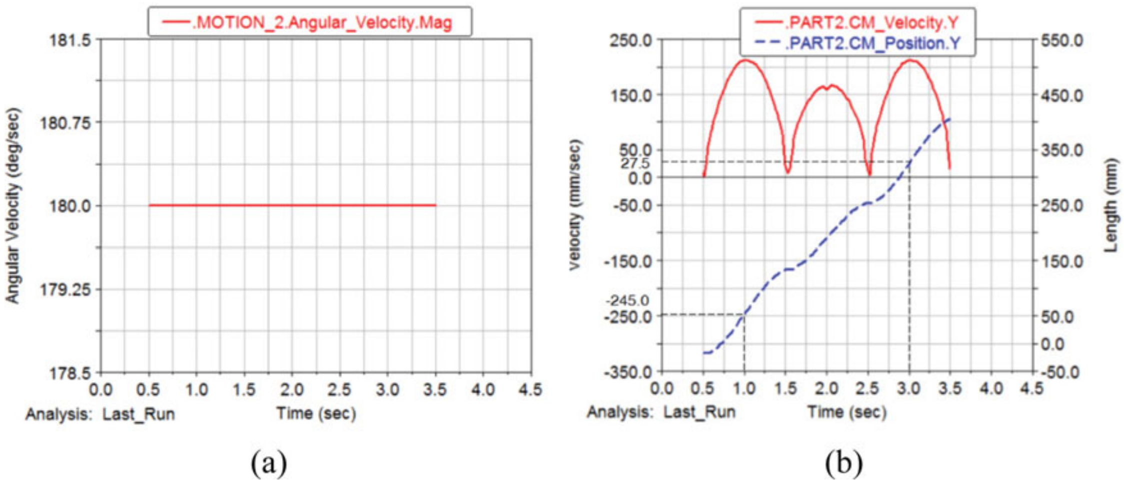

Fig. 19. Input and output of the mobile robot in the wheeled rolling mode: (a) velocity of motor; (b): displacement and velocity of foot 2.

4.7. Somersaulting motion

The somersaulting motion (mode VII in Table I) and turning motion (mode VIII in Table I) are also discovered apart from the five typical motion modes mentioned above. When the mobile robot is in configuration III, it can achieve somersaulting motion.

4.7.1. Gait analysis. Figure 21 shows the locomotion phase of somersaulting mode. Rotating $M1$ clockwise, the robot can achieve somersaulting motion and climb over perpendicular obstacle such as fence.

4.7.2. Stability analysis. The projection view on yz plane of the mobile robot is shown in Fig. 22, based on which, a coordinate system is established. y-axis is along DE (projection of foot 1) and

https://doi.org/10.1017/S0263574718000498 Published online by Cambridge University Press

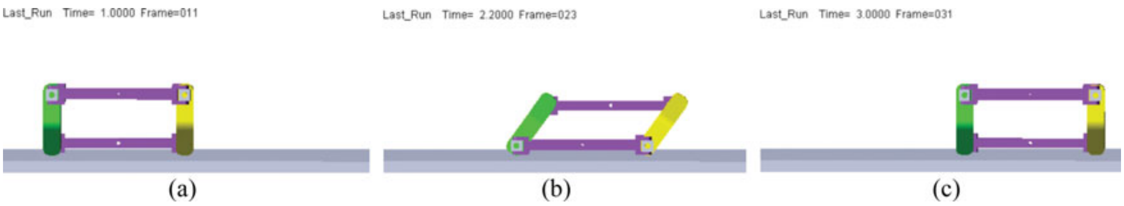

Fig. 20. Simulation process in one cycle in the wheeled rolling mode.

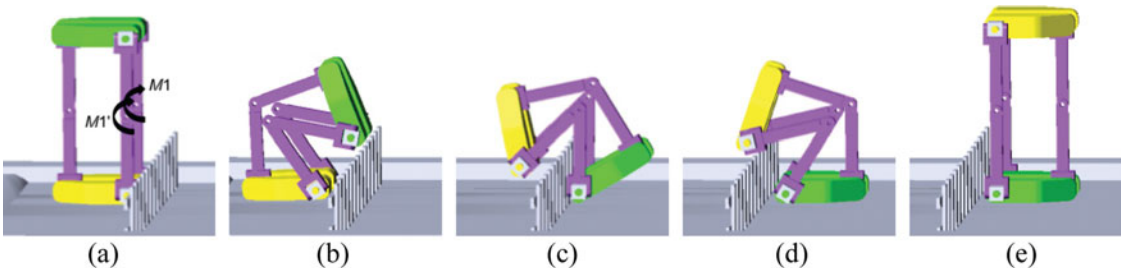

Fig. 21. Somersaulting mode.

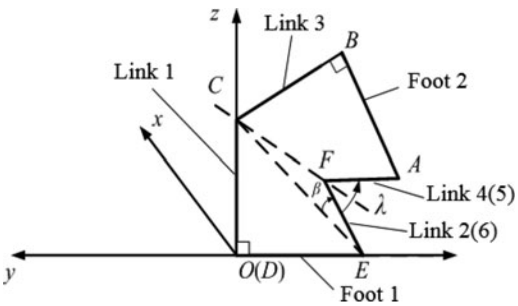

Fig. 22. The projection view on *yz* plane of the mobile robot in the somersaulting mode.

z-axis is along CD (projection of link 1). y_{zmp} can be calculated as

$$
\begin{aligned}
y_{zmp} = \Big\{ &-a\Big\{44g + 11a\ddot{\beta} + 2(-2\dot{\beta}+\omega)^2 + 8a\omega^2\cos\lambda \\
&+ 4 - \{7g + 6a[-\ddot{\beta} + (-2\dot{\beta}+\omega)^2]\}\cos(\lambda-2\beta) + 8\dot{\beta}^2\cos 2(\lambda-2\beta) \\
&+ 40a\ddot{\beta}\cos 2(\lambda-2\beta) - 8\dot{\beta}\omega\cos 2(\lambda-2\beta) + 2\omega^2\cos 2(\lambda-2\beta) \\
&- a\dot{\beta}^2\cos 2\beta - 8a\ddot{\beta}\cos\left(\frac{\pi}{4}+\beta\right) - 8a\dot{\beta}^2\cos\left(\frac{\pi}{4}+\lambda+\beta\right) \\
&- 8a\omega^2\cos\left(\frac{\pi}{4}+\lambda+\beta\right) + 48a\dot{\beta}^2\sin(\lambda-2\beta) - 48a\ddot{\beta}\sin(\lambda-2\beta) - 48a\dot{\beta}\omega\sin(\lambda-2\beta) \\
&+ 12a\omega^2\sin(\lambda-2\beta) + 4g[-6cos\left(\frac{\pi}{4}+\beta\right) \\
&+ 2sin\lambda + 3sin(\lambda-2\beta)] - 4\ddot{\beta}\sin 2(\lambda-2\beta) - a\ddot{\beta}\sin 2\beta + 8a\dot{\beta}^2\sin\left(\frac{\pi}{4}+\beta\right) \\
&- 8a\ddot{\beta}\sin\left(\frac{\pi}{4}+\lambda+\beta\right)\Big\}\Big\} \Big/ \Big\{4\Big\{24g + 2a\omega^2\cos\lambda \\
&+ a[14\ddot{\beta} - 3(-2\dot{\beta}+\omega)^2]\cos(\lambda-2\beta) + a\Big\{-2\ddot{\beta}\cos\left(\frac{\pi}{4}+\beta\right) \\
&+ [6\ddot{\beta} - 7(-2\dot{\beta}+\omega)^2]\sin(\lambda-2\beta) + 2\dot{\beta}^2\sin\left(\frac{\pi}{4}+\beta\right)\Big\}\Big\}\Big\}
\end{aligned}
\tag{21}
$$

https://doi.org/10.1017/S0263574718000498 Published online by Cambridge University Press

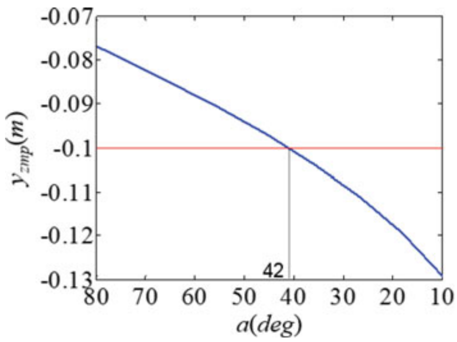

Fig. 23. Plot of ZMP in the somersaulting mode.

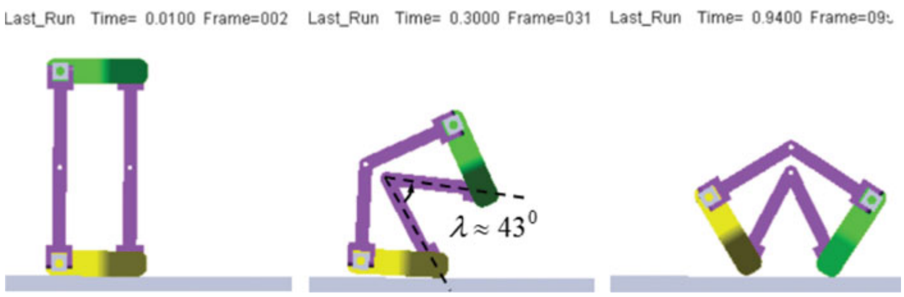

Fig. 24. Simulation result of the mobile robot in the somersaulting mode.

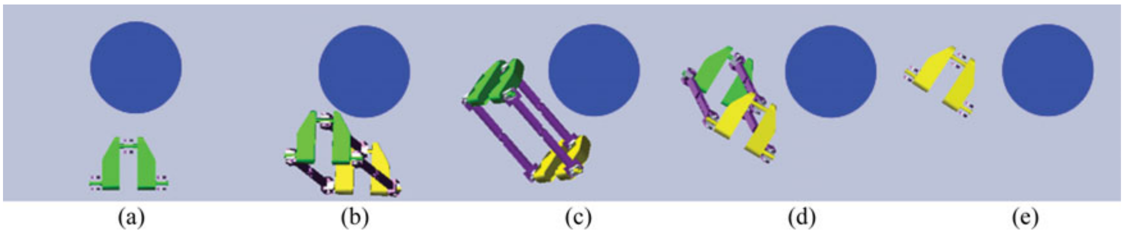

Fig. 25. Turning mode.

The formula of $\dot{\beta}$ and $\ddot{\beta}$ is presented in supplementary material D. The robot in this mode tips over when $y_{zmp} < -a$, and the scale of λ can be got as $\lambda < 42.71°$. The height of the obstacle $H = a \times \cos(\lambda/2) \leq 0.93a$.

The relationship between λ and y_{zmp} is shown in Fig. 23. The simulation result is given in Fig. 24, which verifies the stability analysis.

4.8. Turning motion

The mobile robot can change its moving direction when it is in configuration IV. The mode is called the turning mode (mode VIII in Table I).

4.8.1. Gait analysis. When $M1$ is immobilized, driving $M2$, $M3$, $M4$ to rotate with the same angle [Fig. 25(b)], the robot will achieve turning motion. The steering angle is 45°. After tipping over, change the direction of $M4$ quickly, and the robot will get to its feet under the action of inertia forces and moments, as shown in Fig. 25(d).

The trajectory of the robot in the turning mode is a hexagon, and the maximum radiation of the obstacle $r = \sqrt{3}a$, as shown in Fig. 26.

4.8.2. Stability analysis. Here, only the cases when $\theta_1 = \theta_2, \quad \omega_1 = \omega_2$ are analyzed. The supporting area is a triangle with the side length of a. When going beyond the supporting area, the robot tips

https://doi.org/10.1017/S0263574718000498 Published online by Cambridge University Press

Table II. Size of the robot.

Height	Length	Width	Mass
285 mm	128 mm	236 mm	1.384 kg

Table III. Parameter of motors.

Type	Voltage	Velocity	Moment	Capacity	Mass
DC	12 V	18 *r*/min	30 kg·cm	25 w	95 g

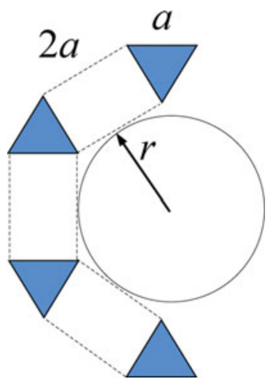

Fig. 26. The trajectory of the robot in the turning mode.

over. x_{zmp} and y_{zmp} are calculated as

$$x_{zmp} = \frac{a\cos\theta_1(q1+q2)}{8[g-2a\omega_1\omega_2\cos\theta_1\cos\theta_2 - a({\omega_1}^2+{\omega_2}^2)\sin\theta_1\sin\theta_2]} \tag{22}$$

$$y_{zmp} = \frac{a(k1+k2+24a{\omega_2}^2\cos\theta_2\sin\theta_2\sin\theta_1)}{24[g-2a\omega_1\omega_2\cos\theta_1\cos\theta_2 - a({\omega_1}^2+{\omega_2}^2)\sin\theta_1\sin\theta_2]} \tag{23}$$

where

$$q1 = 8g - 26a\omega_1\omega_2\cos\theta_1\cos\theta_2$$
$$q2 = a\sin\theta_1[8{\omega_1}^2\sin\theta_2 - (8{\omega_1}^2+13{\omega_2}^2)\sin\theta_2]$$

$$k1 = -8g(\sqrt{3}-3\cos\theta_2) + 2a\omega_1\omega_2\cos\theta_1(8\sqrt{3}-39\cos\theta_2)\cos\theta_2$$
$$k2 = a[8\sqrt{3}({\omega_1}^2+{\omega_2}^2) - 3(13{\omega_1}^2+8{\omega_2}^2)\cos\theta_2]\sin\theta_1\sin\theta_2$$

The input angles when the robot tips over can be obtained by calculating the intersection of the ZMP and the supporting area

$$\begin{cases} {y_{zmp}}^{-1}(\theta_1) = {x_{zmp}}^{-1}(\theta_1) \\ y_{zmp} = -\sqrt{3}x_{zmp} \end{cases} \tag{24}$$

When $\omega = \pi$, the robot can tip over if $\theta_1 = \theta_2 \leq 78.6^\circ$, where $x_{zmp=}0.017$ m and $y_{zmp=}-0.029$ m.

Figure 27 provides the plot of ZMP when $\omega = \pi$ and the CM of the robot. The result implies that the robot can flip over with arbitrary value of ω.

A simulation is carried out to verify the correctness of the calculation, as shown in Fig. 28.

5. Prototype Experiments

A prototype of the mobile robot is designed and fabricated (shown in Figs. 2 and 29) to verify the feasibility of the robot. Seven motors are used to avoid singularity and provide sufficient power.

https://doi.org/10.1017/S0263574718000498 Published online by Cambridge University Press

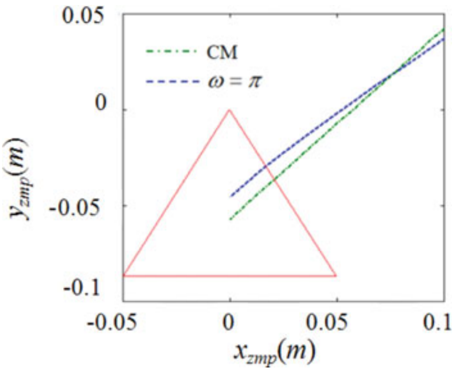

Fig. 27. Plot of ZMP in the turning mode.

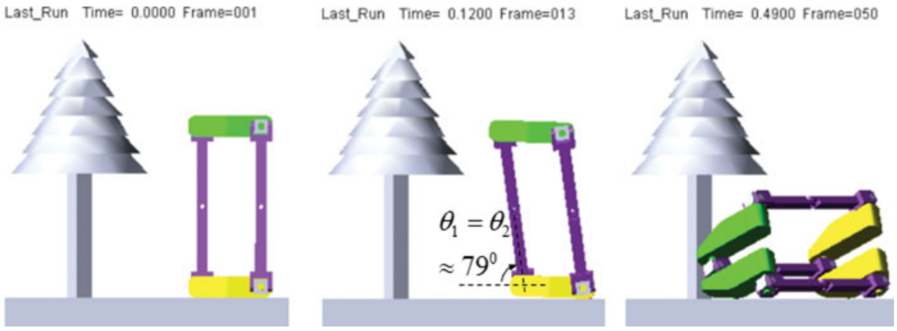

Fig. 28. Simulation result of the mobile robot in the turning mode.

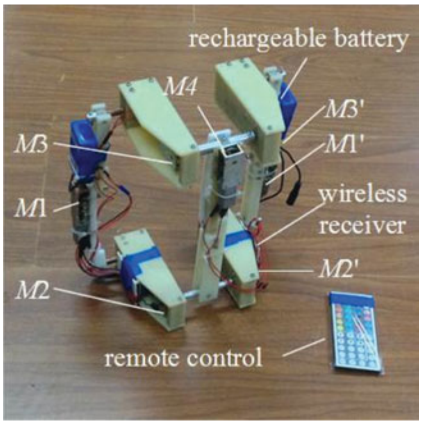

Fig. 29. The prototype of the mobile robot.

The parameters of the prototype are shown in Table II. $M1$ and $M1$' are assembled on R joint $r3$ in limb 3 and R joint $r3$ in limb 2, respectively; $M2$ and $M2$' are mounted on $r5$ of limb 1 and rotate synchronously; $M3$ and $M3$' are assembled on $r1$ of limb 1 and rotate synchronously as well. $M4$ is designed on $r2$ of limb 1. In order to save space and avoid interference, $M2$, $M2$', $M3$ and $M3$' are set on the feet and fastened with U joints. Table III shows the specifications of all the motors.

5.1. Sphere rolling gait

Locking $M4$ and rotating $M1$, $M2$ and $M3$ with the same velocity, the robot rolls in the shape of hexagon throughout the motion. The step size in a half-cycle is 388 mm, as shown in Fig. 30.

https://doi.org/10.1017/S0263574718000498 Published online by Cambridge University Press

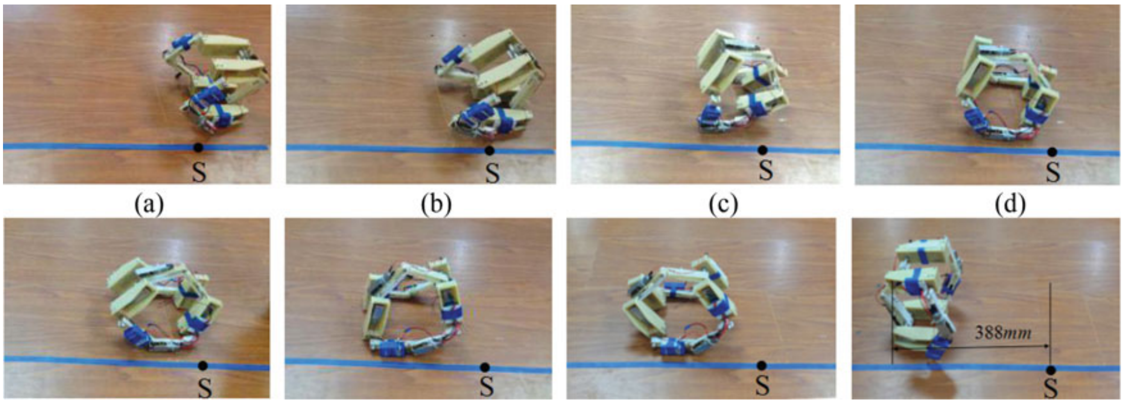

Fig. 30. Sphere rolling gait.

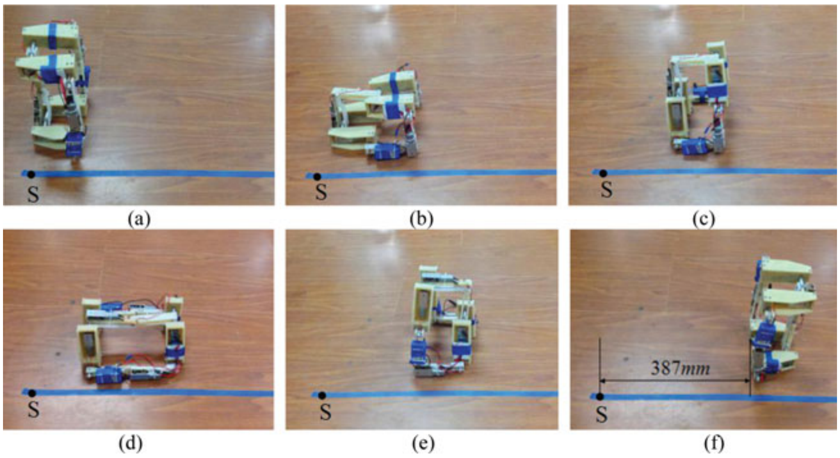

Fig. 31. Tracked rolling gait.

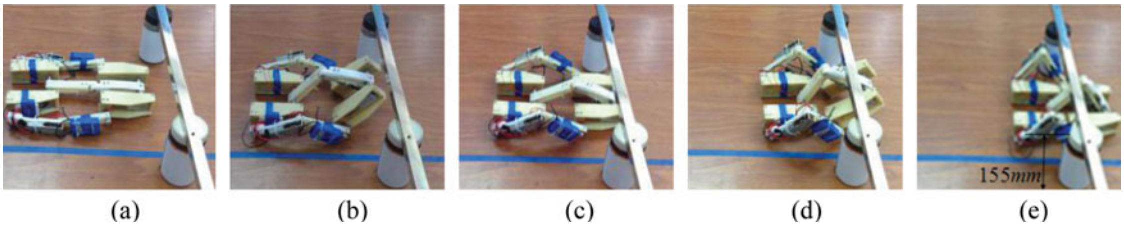

Fig. 32. Squirming gait.

5.2. Tracked rolling gait

The projection view of the mobile robot keeps as a quadrangle in the process of tracked rolling mode, and the trajectory of the prototype is a straight line. The progress forward is 387 mm in a half-cycle, as shown in Fig. 31.

5.3. Squirming gait

In the squirming mode, the robot can go through the bridge with a height limit of 155 mm, as shown in Fig. 32.

5.4. Biped walking gait

Figure 33 shows the process of the biped walking motion. The step size of the robot in the experiment is 337 mm.

https://doi.org/10.1017/S0263574718000498 Published online by Cambridge University Press

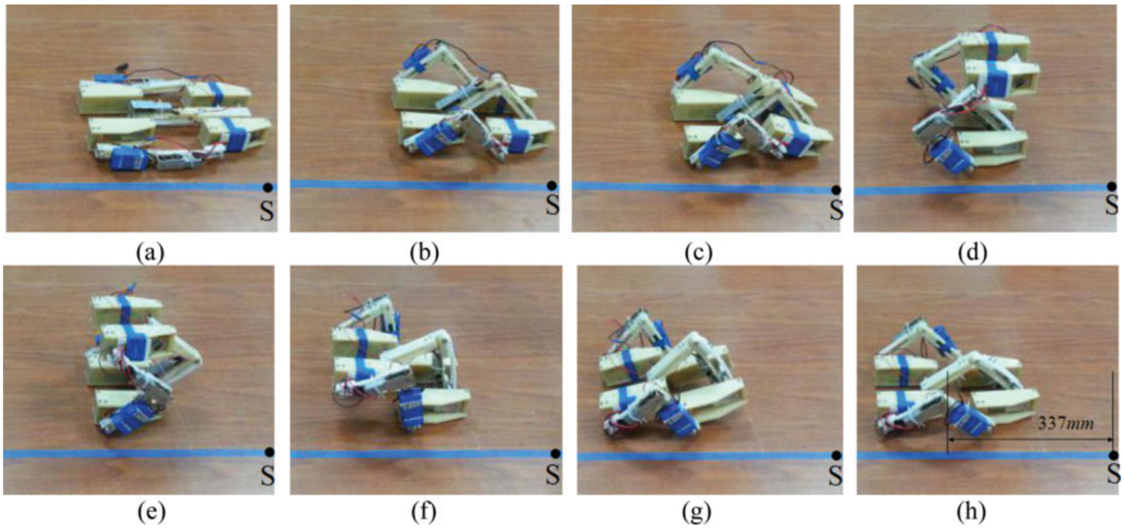

Fig. 33. Biped walking gait.

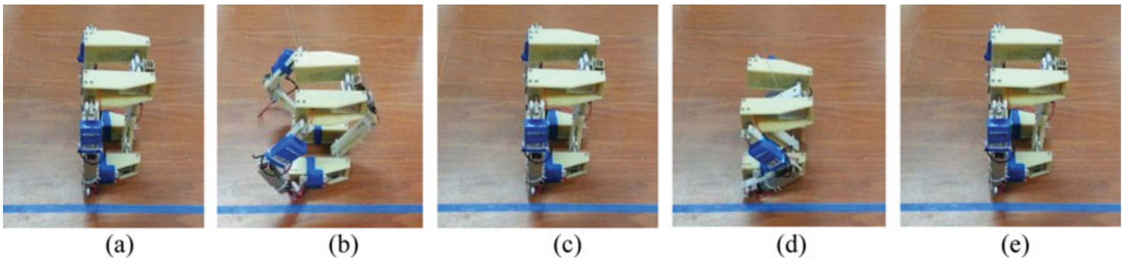

Fig. 34. Folding function.

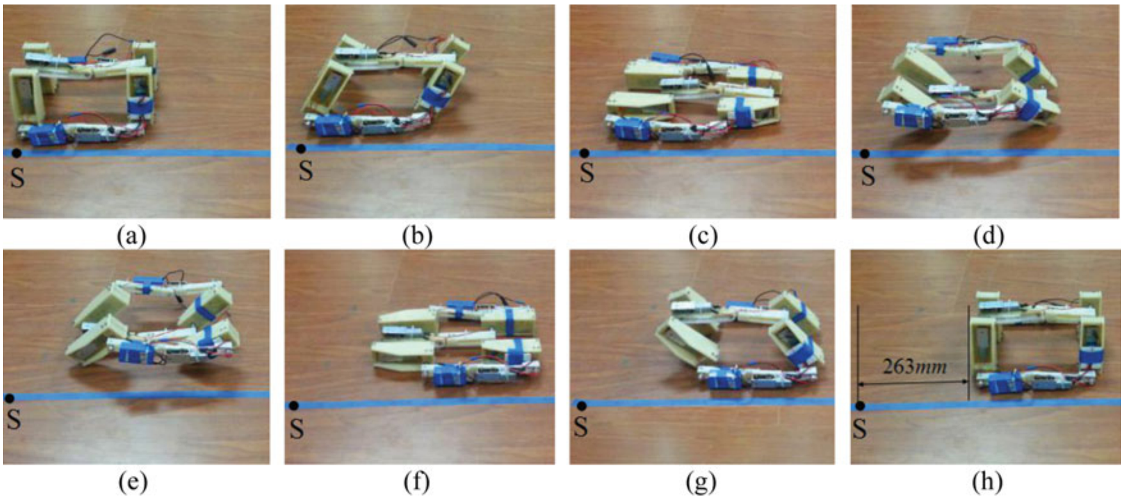

Fig. 35. Wheeled rolling gait.

5.5. Folding function

Figure 34 illustrates the folding function of the robot. The prototype can be folded inward or outward, and the latter one can save more space. The minimum height of the prototype is 145 mm on account of interference of the links.

https://doi.org/10.1017/S0263574718000498 Published online by Cambridge University Press

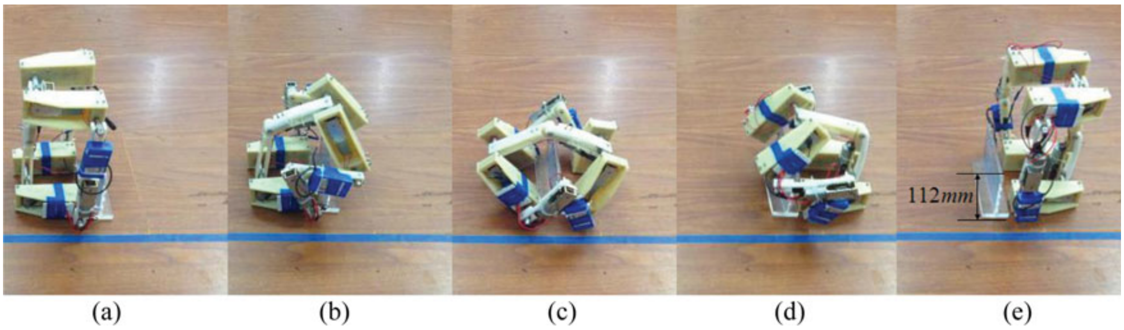

Fig. 36. Somersaulting gait.

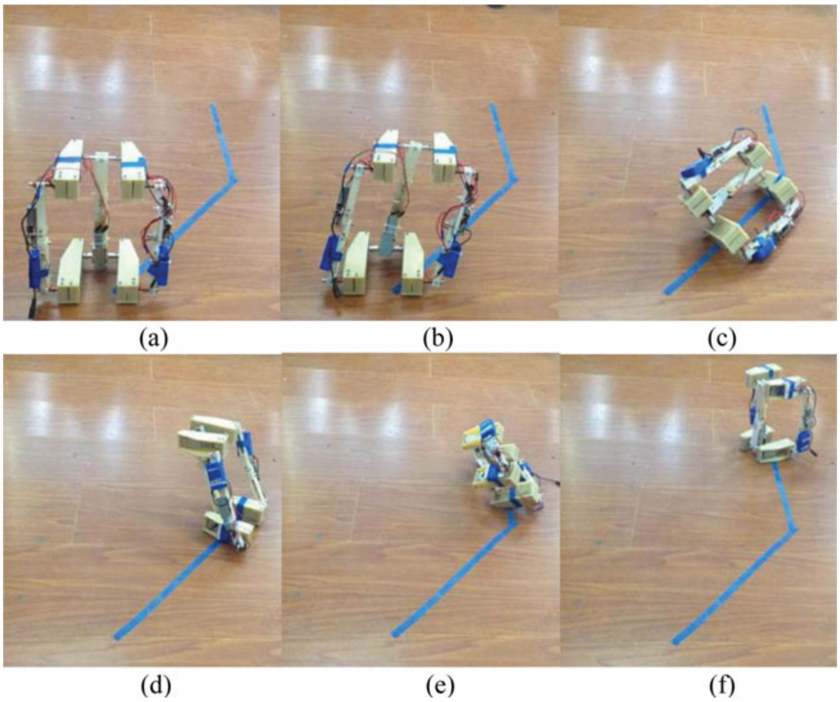

Fig. 37. Turning gait.

5.6. Wheeled rolling gait

Immobilizing $M1$ and $M4$ and letting $M3$ rotate continually, the robot can achieve wheeled rolling motion successively, as shown in Fig. 35. The step length is 263 mm in the experiment. The value is smaller than the result in the simulation, due to the difference of the frictions of the ground and measure error.

5.7. Somersaulting gait

Leaving $M2$, $M3$ and $M4$ be not energized and driving $M1$, consequently, the robot bend down and achieve rolling motion. As shown in Fig. 36, the prototype can climb over the obstacle with the height of 112 mm.

5.8. Turning gait

In the turning mode, the robot can roll in the direction of 45° forward and move along a hexagon in a cycle, as shown in Fig. 37. In this mode, the velocity of $M2$, $M3$ and $M4$ should be equal.

6. Conclusion

A novel reconfigurable tri-prism mobile robot with eight modes has been proposed. The mobility, kinematic, stability analyses have been carried out for the robot in different motion modes. The results

https://doi.org/10.1017/S0263574718000498 Published online by Cambridge University Press

have been verified by both simulations and prototype experiments. This mobile robot integrates the characteristics of sphere robots, squirming robots, tracked robots, wheeled robots and biped robots. The gait of turning and climbing over high obstacles has also been explored. The robot can adapt to different kinds of environment due to its deformability performance and multiple motions modes. In addition, the robot can be folded inward or outward to facilitate storage and transportation.

The tri-prism mobile robot proposed in this paper has potential to be further developed into a launchable robot since it can work no matter which part of the robot touches the ground when landing. The deformation strategy has been developed as follows: operating in wheeled rolling mode on normal road in highest speed; deforming into tracked rolling mode after falling into soft sand and evolving into squirming mode when encountering height restrictions; the biped walking mode is suitable for overcoming discrete barriers and somersaulting motion should be used when coming across high obstacles. After fulfilling tasks, the robot can be folded and stored or transported to other places.

This work provides a solid foundation for further investigation on this mobile robot, including exploring additional mobile modes of the robot using the approaches proposed in refs. [46, 47], optimizing the prototype of the robot to improve its foldability and flexibility, and providing comparisons between theoretical results and experimental results. How to improve the control method of the mobile robot with multiple modes also deserves further investigation. When equipping microcameras and sensors inside the platforms, the robot can be applied to investigate unknown environments such as Mars, battle fields and disaster areas.

Acknowledgments

This work has been supported by National Natural Science Foundation of China (51175030) and Fundamental Research Funds for the Central Universities (2012JBZ002). The first author would like to thank Mr Zhihuai Miao of Harbin Institute of Technology Shenzhen Graduate School and Mr Qiang Ruan of Beijing Jiaotong University, China for their suggestions on the prototype design.

7. Supplementary Material

To view supplementary material for this article, please visit http://dx.doi.10.1017/S0263574718000498.

References

1. J. A. T. Machado and M. F. Silva, "An Overview of Legged Robots," *Proceedings of International Symposium on Mathematical Methods in Engineering*, Ankara, Turquia, MME Press (2006).
2. J. A. Cobano, J. Estremera and P. G. Santos, "Location of legged robots in outdoor environments," *Robot. Auton. Syst.* **56**(9), 751–761 (2008).
3. M. Raibert, K. Blankespoor, G. Nelson and R. Playter, "Bigdog, the rough-terrain quaduped robot," IFAC Proceedings Volumes, **41**(2), (2008), pp. 10822–10825.
4. A. Halme, T. Schonberg and Y. Wang, "Motion Control of a Spherical Mobile Robot," *Proceedings of the 4th IEEE International Workshop on Advanced Motion Control*, Mie, Japan, vol. 1 (1996) pp. 259–264.
5. R. H. Armou and J. F. V. Vincent, "Rolling in nature and robotics: A review," *J. Bionic Eng.* **3**(4), 195–208 (2006).
6. T. Das and R. Mukherjee, "Exponential stabilization of the rolling sphere," *Automatica* **40**(11), 1877–1889 (2004).
7. G. Campion, G. Bastin and B. Dandrea-Novel, "Structural Properties and Classification of Kinematic and Dynamic Models of Wheeled Mobile Robots," IEEE transactions on robotics and automation, **12**(1), (1996), pp. 47–62.
8. S. Hirose, *Biologically Inspired Robots (Snake-like Locomotor and Manipulator)*, (Oxford University Press, Oxford, 1993).
9. K. Togawa, M. Mori and S. Hirose, "Study on Three-Dimensional Active Cord Mechanism Development of ACM-R2," *Proceedings of the IEEE RSJ International Conference on Intelligent Robots and Systems IROS2000*,vol. **3** (2000) pp. 2242–2247.
10. S. Maeda, Y. Hara, R. Yoshida and S. Hashimoto, "Chemical Robot-Design of Self-walking Gel," *Proceedings of the IEEE RSJ International Conference on Intelligent Robots and Systems* (2007) pp. 2150–2155.
11. J. Zhu, D. Sun and S. Tso, "Development of a tracked climbing robot," *J. Intell. Robot. Syst.* **35**(4), 427–443 (2002).

12. R. Volpe, J. Balaram, T. Ohm and R. Ivlev, "The Rocky 7 Mars Rover Prototype," *Proceedings of the IEEE/RSJ International Conference on Intelligent Robots and Systems*, Osaka, Japan, vol. **3** (1996) pp. 1558–1564.
13. Y. G. Kim, J. H. Kwak and D. H. Hong, "Autonomous terrain adaptation and user-friendly teleoperation of wheel-track hybrid mobile robot," *Int. J. Precis. Eng. Manuf.*, **13**(10), 1781–1788 (2012).
14. B. Yamauchi, "PackBot: A Versatile Platform for Military Robotics," *Unmanned Ground Vehicle Technology VI, International Society for Optics and Photonics* (2004) pp. 228–237.
15. M. Guarnieri, I. Takao, E. F. Fukushima and S. Hirose, "HELIOS VIII Search and Rescue Robot: Design of an Adaptive Gripper and System Improvements," *Proceedings of the IEEE/RSJ International Conference on Intelligent Robots and Systems* (2007) 1775–1780.
16. M. Guarnieri and P. Debenest, "Helios 7," *J. Robot. Mechatron.* **141**, 171–177 (2003).
17. M. Guarnieri, P. Debenest, T. Inoh, E. Fukushima and S. Hirose, "Helios VII: A new vehicle for disaster response, mechanical design and basic experiments," *Adv. Rot.*, **19**(8), 901–927 (2005).
18. A. Halme, J. Suomela, T. Schönberg and Y. Wang, "A Spherical Mobile Micro-Robot for Scientific Applications," *Proceedings of* ASTRA, (1996).
19. F. Michaud, D. Létourneau, M. Arsenault, Y. Bergeron and R. Cadrin, "Multi-modal locomotion robotic platform using leg-track-wheel articulations," *Auton. Robot.* **18**(2), 137–156 (2005).
20. P. J. Lewis, N. Flann, M. R. Torrie, E. A. Poulson, T. Petroff and G. Witus, "Chaos: An intelligent ultra-mobile SUGV: Combining the mobility of wheels, tracks, and legs," *Proc. SPIE* **5804**, 427–438 (2005).
21. M. Yim, W. Shen, B. Salemi, D. Rus, M. Moll, H. Lipson, E. Klavins and G. Chirikjian, "Modular Self-reconfigurable robot systems," *IEEE Robot. Autom. Mag.* **14**(1), 43–52 (2007).
22. A. Pamecha, C. Chiang, D. Stein and G. Chirikjian, "Design and Implementation of Metamorphic Robots," *Proceedings of ASME Design Engineering Technical Conference & Computers in Engineering Conference* (1996).
23. C. H. Liu, Y. A. Yao, R. M. Li, Y. B. Tian, N. Zhang, Y. Y. Ji and F. Z. Kong, "Rolling 4R linkages," *Mech. Mach. Theory*, **48**, 1–14 (2012).
24. Z. H. Miao, Y. A. Yao and Y. B. Tian, "A type of novel usage of 4U parallelogram mechanisms-designed as a whole to be biped walking mechanism," *Robot*, **33**(4), 394–404 (2011).
25. Z. H. Miao and Y. A. Yao, "A rolling 6U parallel mechanism," *Frontiers Mech. Eng. China* **6**(1), 96–98 (2011).
26. S. Hirose, K. Homma, S. Matsuzawa and S. Hayakawa, "Parallel Link Walking Vehicle and its Basic Experiments," *Proceedings of the 6th Symposium on intelligent Mobile Robots* (1992) pp. 7–8.
27. G. Reg Dunlop, *Foot Design for a Large Walking Delta Robot. Experimental Robotics VIII*, (Springer, Berlin Heidelberg) pp. 602–611 (2003).
28. C. J. Zhang and Y. W. Li, "A new walking robot based on 3-RPC parallel mechanism," *J. Mech. Eng.* **47**, 25–30 (2011).
29. C. Yan and Y. Zhou, "Two-fold symmetrical 6r foldable frame and its bifurcations," *Int. J. Solids Struct.* **46**(25), 4504–4514 (2009).
30. J. S. Dai and J. J. Rees, "Mobility in metamorohic mechanisms of foldable/ erectable kinds," *ASME Trans. J. Mech. Des.* **121**(3), 375–382 (1999).
31. C. Galletti and P. Fanghella, "Single-loop kinematotropic mechanisms," *Mech. Mach. Theory*, **36**(6), 743–761 (2001).
32. C. C. Lee and J. M. Herve, "Discontinuously Movable 8R Mechanisms with an Infinity of Bifurcations," *Proceedings of 12th IFToMM Word Congress*, Besancon, France (2007).
33. X. Kong, "Type synthesis of 3-DOF parallel manipulators with both a planar operation mode and a spatial translational operation mode," *ASME J. Mech. Robot.* 5(4), 041015 (2013).
34. X. Kong and C. Huang, "Type Synthesis of Single-DOF Single-loop Mechanisms with Two Operation Modes," *Proceedings of ASME/IFToMM International Conference on Reconfigurable Mechanisms and Robots* (2009) pp. 136–141.
35. X. Kong and Y. Jin, "Type synthesis of 3-DOF multi-mode translational/spherical parallel mechanisms with lockable joints," *Mech. Mach. Theory*, **96**(2), 323–333 (2016).
36. K. T. Zhang, Y. F. Fang and H. R. Fang, "Design and analysis of a rover mechanism based on metamorphic principle," *J. Beijing Univ. Aeronau. Astronaut.* **33**(7), 838–841 (2007).
37. N. Wang, Y. Fang and D. Zhang, "A spatial single loop kinematotropic mechanism used for biped/wheeled switchable robots," *Int. J. Mech. Mater. Des.* **11**(3), 287–299 (2015).
38. X. L. Ding and K. Xu, "Design and analysis of a novel metamorphic wheel-legged rover mechanism," *J. Central South Univ.* **40**(1) 91–101 (2009).
39. Z. Dai and J. Sun, "A biomimetic study of discontinuous-constraint metamorphic mechanism for gecko-like robot," *J. Bionic Eng.* **4**(2), 91–95 (2007).
40. Y. B. Tian, Y. A. Yao and J. Y. Wang, "A rolling 8-bar linkage mechanism," *J. Mech. Robot.* **7**(4), 041002 (2014).
41. J. Wang, Y. Yao and X. Kong, "A rolling mechanism with two modes of planar and spherical linkages," *Proc. Inst. Mech. Eng. Part C: J. Mech. Eng. Sci.* **230**(12), 2110–2123 (2016).
42. Z. Huang, J. Liu and D. Zeng, "A general methodology for mobility analysis of mechanisms based on constraint screw theory," *Sci. China Series E: Technol. Sci.* **52**(5), 1337–1347 (2009).
43. Z. Huang and Y. F. Fang, "Kinematic characteristics analysis of 3 DOF in-parallel actuated pyramid mechanism," *Mech. Mach. Theory*, **31**(8), 1009–1018 (1996).

44. X. Kong and C. M. Gosselin, *Type Synthesis of Parallel Mechanisms*, (Springer Publishing Company, Incorporated, 2007).
45. M. Vukobratovic and B. Borovac, "Zero-moment point-thirty five years of its life," *Int. J. Humanoid Robot.* **1**(1), 157–173 (2004).
46. D. R. Walter, M. L. Husty and M. Pfurner, "A complete kinematic analysis of the SNU 3-UPU parallel robot," *Contemp. Math.* **496**, 331 (2009).
47. X. Kong, "Reconfiguration analysis of a 3-DOF parallel mechanism using Euler parameter quaternions and algebraic geometry method," *Mech. Mach. Theory*, **74**, 188–201 (2014).